

Modeling radio communication blackout and blackout mitigation in hypersonic vehicles

Madhusudhan Kundrapu¹, John Loverich², Kristian Beckwith³, Peter Stoltz⁴
Tech-X Corporation, Boulder, CO, 80303, USA

Alexey Shashurin⁵ and Michael Keidar⁶
The George Washington University, Washington, DC, 20052, USA

A procedure for the modeling and analysis of radio communication blackout of hypersonic vehicles is presented. A weakly ionized plasma generated around the surface of a hypersonic reentry vehicle traveling at Mach 23 was simulated using full Navier-Stokes equations in multi-species single fluid form. A seven species air chemistry model is used to compute the individual species densities in air including ionization - plasma densities are compared with experiment. The electromagnetic wave's interaction with the plasma layer is modeled using multi-fluid equations for fluid transport and full Maxwell's equations for the electromagnetic fields. The multi-fluid solver is verified for a whistler wave propagating through a slab. First principles radio communication blackout over a hypersonic vehicle is demonstrated along with a simple blackout mitigation scheme using a magnetic window.

¹ Associate Research Scientist

² Research Scientist

³ Research Scientist

⁴ Vice President

⁵ Research Scientist, Mechanical and Aerospace Engineering

⁶ Professor, Mechanical and Aerospace Engineering

Nomenclature

A	= amplitude of oscillation
\vec{B}	= magnetic field, T
\vec{B}_0	= background static magnetic field, T
c	= speed of light, m/s
c_p	= specific heat at constant pressure, J/kg K
c_v	= specific heat at constant volume, J/kg K
\vec{E}	= electric field, V/m
e	= total (internal+kinetic+chemical) energy of the fluid , J/m ³
	= electron
f	= number of degrees of freedom
	= frequency, Hz
H	= enthalpy of formation, J/particle
I	= identity matrix
k_T	= thermal conductivity, W/m K
k	= wave number
k_B	= Boltzmann constant, J/K
m	= mass of a unit species, kg
M	= molecular weight, g/mol
q	= charge of a unit species, C
Q	= internal energy exchange rate per unit volume, W/m ³
Q_{EM}	= energy density of the electromagnetic wave, J/m ³
R	= gas constant, J/kg K
\vec{R}	= momentum exchange rate per unit volume, N/m ³
t	= time, s
T	= temperature, K
\vec{u}	= velocity, m/s

γ	= gas constant (c_p/c_v)
μ	= dynamic viscosity, N s/m ²
	= reduced mass, kg
ρ	= density, kg/m ³
τ	= stress tensor, N/m ²
σ	= collision diameter, m
ϵ_0	= permittivity of free space, F/m
ζ	= collision time, s
n_α	= species number density, 1/m ³
Ω	= collision integral
Ω_{ce}	= electron cyclotron frequency, radians/s
Ω_{ci}	= ion cyclotron frequency, radians/s
Ω_{pe}	= electron plasma frequency, radians/s
Ω_{pi}	= ion plasma frequency, radians/s
Subscripts	
α	= index of a species
i	= index of species other than the species α
Superscripts	
T	= transpose

I. Introduction

Hypersonic vehicles are subjected to severe aerothermal heating due to the formation of shock waves in front of the vehicle. Flow Mach numbers exceeding four are classified as hypersonic[1] and in this regime the kinetic energy of the flow, when converted to internal energy through the shock provides a significant increase in the fluid temperature. The temperatures quite often exceeds the dissociation and ionization limits of the flow species and results in the formation of a weakly ionized plasma layer around the vehicle. The electrons in the plasma layer may interrupt the propagation of radio frequency electromagnetic waves if the plasma electron oscillation frequency exceeds that

of the electromagnetic wave frequency. This phenomenon is commonly called radio communication blackout. For instance, a 1.6 GHz radio wave will be interrupted by a plasma layer of density of 3.5×10^{16} . Blackout mitigation is an important requirement for the design of hypersonic vehicles, especially for those vehicles in steady state hypersonic flight such as those envisioned by NASA and the US Air Force. A few mitigation mechanisms described in the literature are the magnetic window[13, 24, 32], electrophilic fluid injection[2], wave frequency modification, aerodynamic shape modification, $E \times B$ drift[21, 22], resonant transmission[33], time varying magnetic field[3] and electron acoustic wave transmission[34]. The magnetic window uses a static magnetic field to convert the free space radio wave to a whistler wave in the plasma.[23] Electrophilic injection uses an electrophilic substance injected into the fluid to decrease the electron density. Wave frequency and aerodynamic shape modification have design limitations so may be impractical in many cases. The $E \times B$ drift accelerates the ions in the layer there by decreasing the plasma density near the antenna. Resonant transmission uses surface wave resonance to enhance transmission through the plasma layer. The time varying magnetic field approach uses the hall effect to expel ions. Electron acoustic wave transmission works by converting the wave into an electron acoustic wave in the plasma layer. Numerical simulations of blackout mitigation techniques are valuable during the design phase of hypersonic vehicles.

Radio communication blackout modeling of aerospace vehicles with full wave electromagnetics has been investigated by several groups with many different codes. Takahashi[14, 15] uses a CFD tool to compute the plasma distribution and then a FDTD solver with a modified permittivity to account for the presence of a plasma. Thoma[32] used the high density FDTD PIC code LSP to investigate the magnetic window with a horn antenna surrounded by an assumed plasma distribution. Visbal[4] uses a multi-fluid electromagnetic approach to modeling radio communication blackout on an over-set mesh, without an investigation of steady magnetic field effects.

The scope of this paper is to show the modeling approach that works for realistic vehicles in complex geometries and can be used to simulate the feasibility of blackout mitigation devices for hypersonic vehicles. The RAM C reentry vehicle is used for this demonstration as there is significant experimental data for comparison. USim[28, 30, 31], a commercial code developed by Tech-X Cor-

poration for general fluid plasma modeling on unstructured grids, is used for all simulations in this paper. This paper is organized as follows: (1) Modeling and simulation of the multi-species hypersonic flow over the RAM C reentry vehicle to obtain the plasma density distribution (2) Validation of the plasma density distribution with the results from literature (3) Modeling of electromagnetic wave propagation into the plasma and validation with the dispersion relation and (4) Finally, the propagation of plane EM wave on to the vehicle's surface through the plasma layer using a magnetic window and the whistler wave conversion.

II. Mathematical formulation

A. Bulk fluid transport

A generalized model for simulating the compressible flow with reacting multi-species is given in this section. The Navier-Stokes equations in conservative form Eqs. (1)–(3) were used for the conservation of fluid mass, momentum, and total energy respectively. The total energy e in Eq. (3) is the sum of internal energy, kinetic energy and the chemical energy of the fluid. The fluid was assumed to be Newtonian and obeys the Stoke's hypothesis of zero bulk viscosity. Further, the fluid obeys the ideal gas law for equation of state.

$$\frac{\partial \rho}{\partial t} + \nabla \cdot (\rho \vec{u}) = 0 \quad (1)$$

$$\frac{\partial (\rho \vec{u})}{\partial t} + \nabla \cdot (\rho \vec{u} \vec{u} + pI) = \nabla \cdot \tau \quad (2)$$

$$\frac{\partial (e)}{\partial t} + \nabla \cdot (\vec{u}(e + p)) = \nabla \cdot (\tau \cdot \vec{u}) + \nabla \cdot (k_T \nabla T) \quad (3)$$

where,

$$\rho = \sum_i n_i m_i \quad (4)$$

$$p = \rho RT \quad (5)$$

$$\tau = -\frac{2}{3}\mu (\nabla \cdot \vec{u}) I + \mu (\nabla \vec{u} + (\nabla \vec{u})^T) \quad (6)$$

$$e = \frac{p}{\gamma - 1} + \frac{1}{2} \rho \vec{u} \cdot \vec{u} + \sum_i n_i H_i \quad (7)$$

and

$$\gamma = \frac{c_p}{c_p - R} \quad (8)$$

B. Species transport

The mass conservation of the individual species in the bulk fluid is satisfied separately for each of the species using Eq. 9. The velocity \vec{u} is same as that of the bulk fluid. The right hand side of Eq. 9 represents the rate of change of species density due to the chemical reactions.

$$\frac{\partial n_i}{\partial t} + \nabla \cdot (\vec{u} n_i) = s_i \quad (9)$$

C. Material properties

The properties viscosity, thermal conductivity and the specific heat of the individual species were obtained from the kinetic theory of gases as given by the Eqs. (11)–(13). The fluid thermal conductivity k and viscosity μ in Eqs. (1)–(3) were obtained using mole fraction averaging while the specific heat c_p was obtained using the mass fraction averaging. The gas constant R was computed using the mole fraction averaged molecular weight.

$$c_{p_i} = \left(\frac{f}{2} + 1 \right) R_i \quad (10)$$

$$\mu_i = \frac{5}{16} \frac{\sqrt{\pi m_i k_B T}}{(\pi \sigma^2 \Omega)} \quad (11)$$

$$k_i = \frac{5}{2} c_{v_i} \mu_i \quad (12)$$

$$c_{v_i} = c_{p_i} - R_i \quad (13)$$

D. Electromagnetic multi-fluid

A multi-fluid model was used for the interaction of radio wave with the plasma. Maxwell's equations were used to solve evolution of electric and magnetic fields. Ampere's law and Faraday's

law are given by Eqs. (14) and (15) respectively. The right hand side of Eq. (14) is the sum of the current densities of the conducting species. The divergence equations (16) and (17) should be satisfied along with the Ampere's and Faraday's laws.

$$\frac{\partial \vec{E}}{\partial t} - c^2 \nabla \times \vec{B} = -\frac{1}{\epsilon_0} \sum_{\alpha} \frac{q_{\alpha} \rho_{\alpha} \vec{u}_{\alpha}}{m_{\alpha}} \quad (14)$$

$$\frac{\partial \vec{B}}{\partial t} + \nabla \times \vec{E} = 0 \quad (15)$$

$$\nabla \cdot \vec{E} = \frac{1}{\epsilon_0} \sum_{\alpha} \frac{q_{\alpha} \rho_{\alpha}}{m_{\alpha}} \quad (16)$$

$$\nabla \cdot \vec{B} = 0 \quad (17)$$

The transport of the multi-fluid system was modeled using the system of equations Eqs. (18)–(20). Index α is for any fluid. The first terms on the RHS of Eq.(19) the electric and magnetic Lorentz forces. The third term is the net momentum exchange with the remaining fluids in the system.[25] The first term on the RHS of Eq.(20) is for Joule heating and the fourth and fifth terms are kinetic energy and internal energy exchange terms respectively.[25]

$$\frac{\partial \rho_{\alpha}}{\partial t} + \nabla \cdot (\rho_{\alpha} \vec{u}_{\alpha}) = 0 \quad (18)$$

$$\frac{\partial (\rho_{\alpha} \vec{u}_{\alpha})}{\partial t} + \nabla \cdot (\rho_{\alpha} \vec{u}_{\alpha} \vec{u}_{\alpha} + p_{\alpha} I) = \frac{\rho_{\alpha}}{m_{\alpha}} q_{\alpha} \left(\vec{E} + \vec{u}_{\alpha} \times \vec{B} \right) + \nabla \cdot \tau_{\alpha} + \vec{R}_{\alpha} \quad (19)$$

$$\frac{\partial (e_{\alpha})}{\partial t} + \nabla \cdot (\vec{u}_{\alpha} (e + p_{\alpha})) = \frac{\rho_{\alpha}}{m_{\alpha}} q_{\alpha} \vec{u}_{\alpha} \cdot \vec{E} + \nabla \cdot (\tau_{\alpha} \cdot \vec{u}_{\alpha}) + \nabla \cdot (k_{\alpha} \nabla T_{\alpha}) + \vec{V}_{\alpha} \cdot \vec{R}_{\alpha} + Q_{\alpha} \quad (20)$$

where,

$$\vec{V}_{\alpha} = \left(\sum_i \rho_i \vec{u}_i \right) / \sum_i \rho_i \quad (21)$$

$$\vec{R}_\alpha = - \sum_i \frac{\rho_\alpha}{m_\alpha} \mu_{\alpha i} \zeta_{\alpha i}^{-1} (\vec{u}_\alpha - \vec{u}_i) \quad (22)$$

and

$$Q_\alpha = - \sum_i 3k_B \frac{\rho_\alpha}{m_\alpha} [\mu_{\alpha i} / (m_\alpha + m_i)] \zeta_{\alpha i}^{-1} (T_\alpha - T_i) \quad (23)$$

importantly, this model describes electromagnetic wave propagation in free space (when the charged species densities are zero) and in a conducting fluid (when the charged species densities are non-zero). In particular it describes reflection of electromagnetic waves off of an over-dense plasma as well as electromagnetic wave propagation in a plasma including the changes caused by external magnetic fields. The model is more complete to that of magnetohydrodynamics (MHD) and can be thought of as MHD without the assumption of quasi-neutrality, without the assumption that the light wave is infinitely fast and by using the full Ohm's law, (including electron inertia) in the MHD system. Restricting ourselves to two-fluids for the moment (electrons and ions only), 4 parameters that can be derived from this model, will be important in determining the electromagnetic wave propagation characteristics in the plasma. The first is the electron plasma frequency

$$\Omega_{pe} = \sqrt{\frac{n_e q_e^2}{m_e \epsilon_0}} \quad (24)$$

the second is the electron cyclotron frequency

$$\Omega_{ce} = \frac{q_e B_0}{m_e} \quad (25)$$

followed by the ion plasma frequency

$$\Omega_{pi} = \sqrt{\frac{n_i q_i^2}{m_i \epsilon_0}} \quad (26)$$

and the ion cyclotron frequency

$$\Omega_{ci} = \frac{q_i B_0}{m_i} \quad (27)$$

These parameters will be used in the discussion of the whistler wave.

E. Solution methodology

The equation systems given in Sec. II were solved using a generalized unstructured grid finite volume solver, USim[28, 30, 31]. Though multi-fluid electromagnetic solvers have been developed

throughout the years by several researchers [11, 12, 18–20, 29, 35, 36], the present solver is the first solver using an unstructured formulation and running on an unstructured grid[30] as prior codes were based on multi-block logically Cartesian grids. The flux reconstruction on the cell faces was carried out using second order accurate Monotonic Upstream-Centered Scheme for Conservation Laws (MUSCL)[8]. The right and left fluxes on the cell faces were obtained by extrapolating the cell centered gradient of the conserved variable. The spurious oscillations that may arise due to the flux reconstruction are limited using flux limiters such as Van-Leer limiter.[8] The cell centered gradient was computed using the weighted least squares method. A second degree polynomial was considered in this work. The actual flux on the cell face was then obtained using an approximate Riemann flux. In this work HLLC approximate Riemann flux[9] was considered for the fluid equations while full wave flux was chosen for the Maxwell’s equations. The diffusion fluxes were evaluated by computing the least squares gradient on the cell faces and then performing a surface integral according to the Gauss divergence theorem. Reaction rates were integrated using the Boost ODE integrator[40]. The left and right hand side of the Eqs. (1)–(9), (14), and (15) were evaluated separately and added together and then integrated in time using Runge-Kutta method. A third order RK integration scheme was used. Operator splitting was used for the reaction terms and super time stepping for the diffusion terms.

III. Validation of the results

A. Reactive flow simulation

The simulation was performed for a velocity of 7650 m/s , density $2.816 \times 10^{-4}\text{ kg/m}^3$ and temperature 244.3 K . These values correspond to an altitude of 61 km . The air species N_2 , O_2 , N , O , NO , NO^+ , and e (electron) were considered for the reaction chemistry and the reaction rates were considered from the Ref. [5]. The unstructured grid used for the simulation was shown in Fig. (1). Cubit [39] grid generation software was used for the grid generation. The contour flood represents the area of cells in m^2 . The average edge lengths vary from around 0.5 mm at the nose cap region to 1 mm on the lateral surface.

Flow enters the domain from the top boundary of Fig. 1. An axisymmetric boundary condition

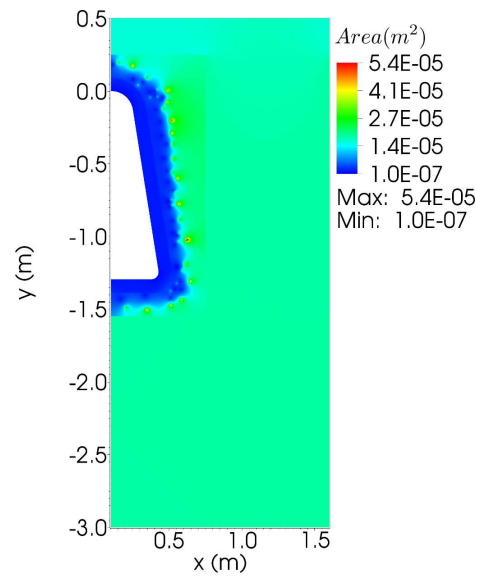


Fig. 1 The unstructured grid used for the simulation. The contour flood represents the cell area.

was imposed on the axis (left boundary). On that wall, a standard no slip and radiation equilibrium temperature were imposed. Outflow boundary conditions were used on the remaining boundaries. The temperature and electron density distributions are shown in Fig. 2. The peak values of average temperature and the electron density are 21860 K and $1.18 \times 10^{20} \text{ m}^{-3}$ respectively existing in the stagnation region. Figure 3 shows the comparison of the surface and peak electron densities in the plasma layer with the reflectometer measurements presented in Ref. [6]. The measurements represent the time averaged values of the electron density measured using 15 reflectometers of four different frequencies placed at four stations on the wall of RAM C. The cut-off densities associated with the four frequencies are 1.52×10^{19} , 1.25×10^{18} , 1.37×10^{17} , and $1.54 \times 10^{16} \text{ m}^{-3}$ respectively.[7] The first station was located at 0.0457 m from the noscap tip. The remaining three stations locations along with the measured peak densities are shown by squares in the figure. The dashed curve represents the curve fit of the measured data points. The bottom most curve is the surface density distribution while the top most curve is the peak density of electrons in the plasma layer of Fig.2(b). The peak values of the simulation are about three times the values from the measurements. Inclusion of radiation losses from the plasma and the diffusion of electrons in the simulation could decrease the density to some extent. Moreover, the comparison shows a good agreement in terms

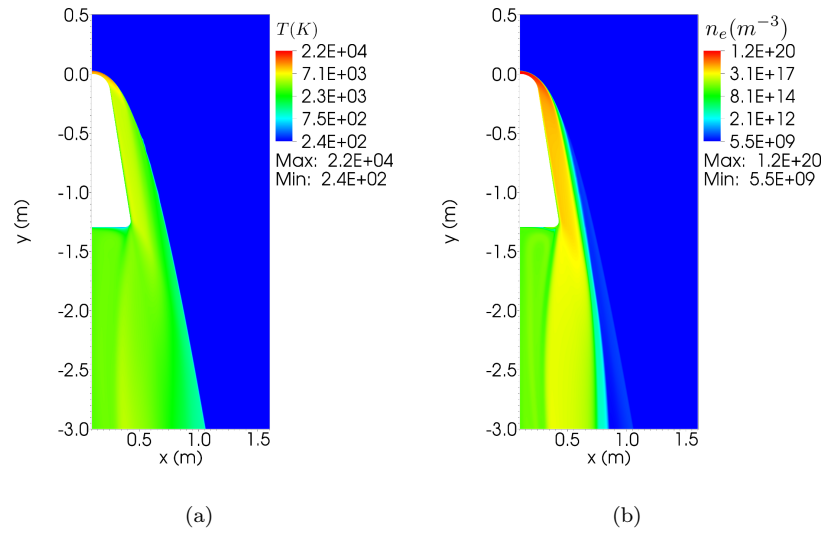


Fig. 2 Flow parameters on RAM C. (a) Temperature distribution and (b) electron number density distribution.

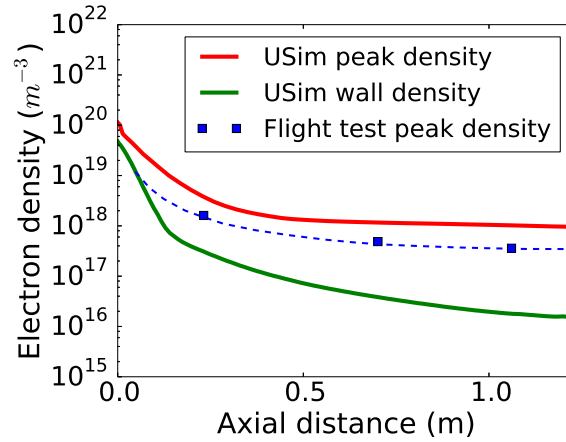


Fig. 3 Validation of the electron density in the plasma layer of RAM C. The top and bottom curves are peak density and surface density respectively. The middle curve is the averaged peak density measurements from Ref.[6]

of the trend and in the design point view, the higher values of the simulation to this extent are acceptable in terms of the factor of safety. The wall densities are well below the peak values, for the simple reason that the wall temperature is much below the boundary layer temperature.

B. Dispersion relation for waves parallel to the magnetic field

The magnetic window approach to radio communication blackout mitigation takes advantages of special properties of electromagnetic wave propagation in plasmas in the presence of a magnetic field.

A derivation of the whistler wave (as well as many other plasma waves) can be found in many plasma physics text books including [37]. In the case below, the dispersion relation is derived from the two-fluid electromagnetic plasma model and written in terms of plasma parameters, $\Omega_{ce}, \Omega_{ci}, \Omega_{pe}, \Omega_{pi}$ and the speed of light c , the results are given as follows. The R-Mode dispersion relation is given by

$$k^2 = \frac{w^2 (w^2 + w(\Omega_{ci} - \Omega_{ce}) - \Omega_{ce}\Omega_{ci} - \Omega_{pe}^2 - \Omega_{pi}^2)}{c^2(w - \Omega_{ce})(w + \Omega_{ci})} \quad (28)$$

ignoring ion motion we get

$$k^2 = \frac{w (w^2 - w\Omega_{ce} - \Omega_{pe}^2)}{c^2(w - \Omega_{ce})} \quad (29)$$

The L-Mode dispersion relation is given by

$$k^2 = \frac{w^2 (w^2 + w(\Omega_{ce} - \Omega_{ci}) - \Omega_{ce}\Omega_{ci} - \Omega_{pe}^2 - \Omega_{pi}^2)}{c^2(w + \Omega_{ce})(w - \Omega_{ci})} \quad (30)$$

ignoring ion motion we get

$$k^2 = \frac{w (w^2 + w\Omega_{ce} - \Omega_{ce}\Omega_{pe}^2)}{c^2(w + \Omega_{ce})} \quad (31)$$

Fig.4 shows the frequency vs wave number plotted for the electromagnetic wave in a plasma without a background magnetic field. At all frequencies below the plasma frequency the wave is evanescent. By adding a magnetic field the dispersion relation changes and the wave can propagate through the plasma at frequencies below the electron cyclotron frequency. Fig.5 shows the frequency vs wave number plotted for the R-Mode and L-Mode waves in non-dimensional units in a plasma with a background magnetic field. The background field can be adjusted so that the signal can propagate through the plasma as a whistler wave which is the magnetic window.

The Fig.6 shows the EM wave propagation in a neutral fluid. A plane wave was excited from the left boundary with the components $E_y = c a_0 \sin(2\pi ft)$ and $B_z = E_y/c$. The frequency of the wave was 1.6 GHz. Uninterrupted propagation of the wave can be clearly seen. A uniform plasma slab of thickness 0.3 m was then added in the domain at $x = -0.15$ m. The plasma density was 10^{19} m^{-3} . Since the frequency of the plasma, 28.4 GHz is much greater than the wave frequency, the wave was completely reflected by the plasma. Figure 7 shows the reflection of electric and magnetic

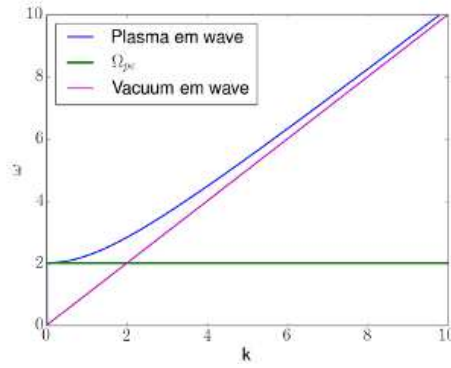


Fig. 4 Dispersion graph for electromagnetic waves traveling in a plasma with no background magnetic field, frequency vs wave number in normalized units. The vacuum electromagnetic wave is provided for comparison. Notice that below the plasma frequency the electromagnetic wave in the plasma does not propagate. This is the reason for radio communication blackout.

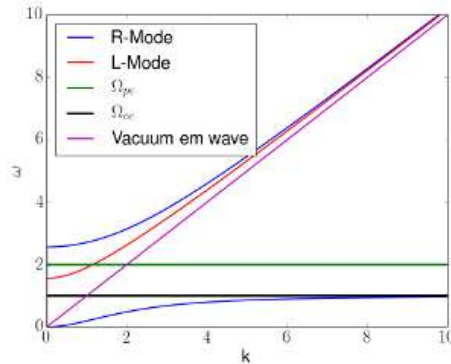


Fig. 5 Dispersion graph for electromagnetic waves traveling parallel to the magnetic field, frequency vs wave number in normalized units. The R-mode wave has two branches, the lower frequency branch which propagates below the plasma frequency is known as the whistler wave. The whistler wave has a cutoff at the electron cyclotron frequency. In the presence of a magnetic field then it is possible for the electromagnetic wave to penetrate the over-dense plasma. The electron cyclotron frequency must be greater than the signal frequency and this puts a lower bound on the magnetic field strength that should be used.

fields. E_y and B_z are shown in Fig. 8(a) and 8(b) respectively. The amplitudes of the electric and magnetic fields doubled since a standing wave is formed upon reflection from the plasma slab. The figure also shows the simulation accuracy of the two-fluid solver.[10, 17]

A constant magnetic field of B_{0x} 1 T was applied in the domain to create a magnetic window

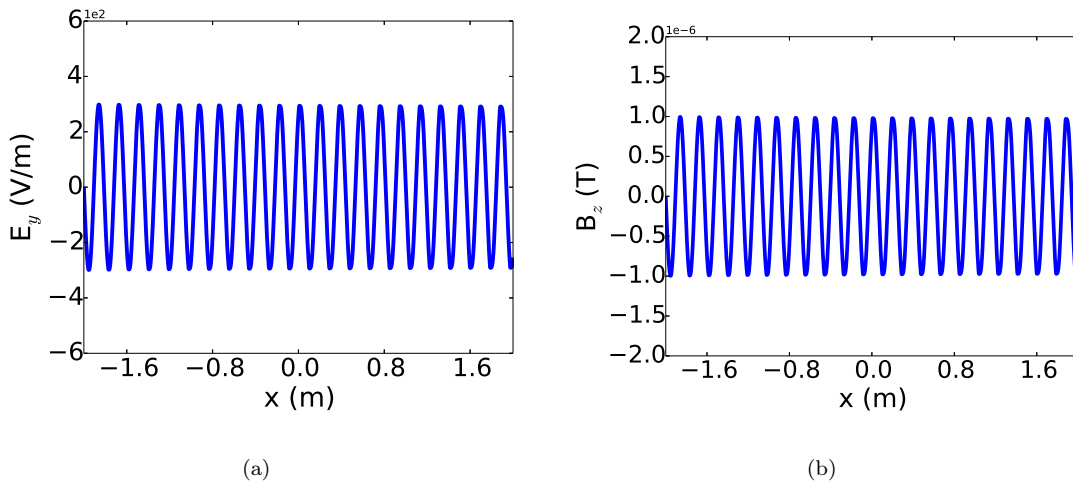


Fig. 6 The (a) y component of electric field and the (b) z component of the magnetic field in the EM wave of frequency 1.6 GHz traveling in neutral fluid.

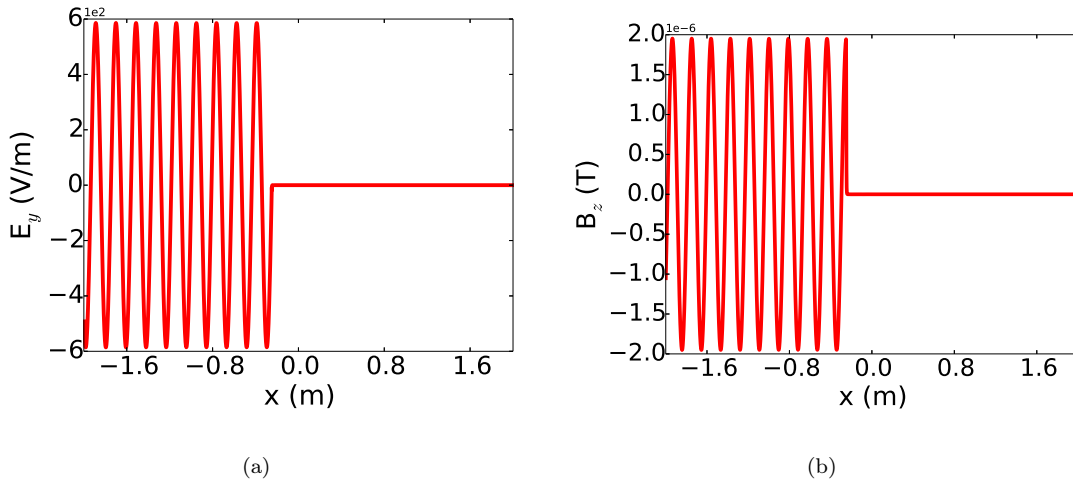


Fig. 7 The (a)y component of electric field and the (b) z component of the magnetic field of the EM wave of frequency 1.6 GHz traveling in a domain with plasma slab of thickness 0.3 m. The slab starts from $x = -0.15$ m. The wave is completely reflected by the plasma hence no propagation in the plasma and beyond the slab.

for the propagation of the wave in whistler mode through the plasma. Figure 8 shows the wave components E_y . The whistler wave's accuracy is compared with the analytical solution obtained from the dispersion theory. The Dispersion relation shows that the wave number of the whistler wave in the plasma slab is 23.89. The Fourier transform of the wave in the spatial domain gives the wavenumber spectrum. The Fourier transform E_x in Fig.8 is shown in Fig.9. The first peak is located around $k = 5.33$ and the second peak around $k=23.89$. The first peak represents the

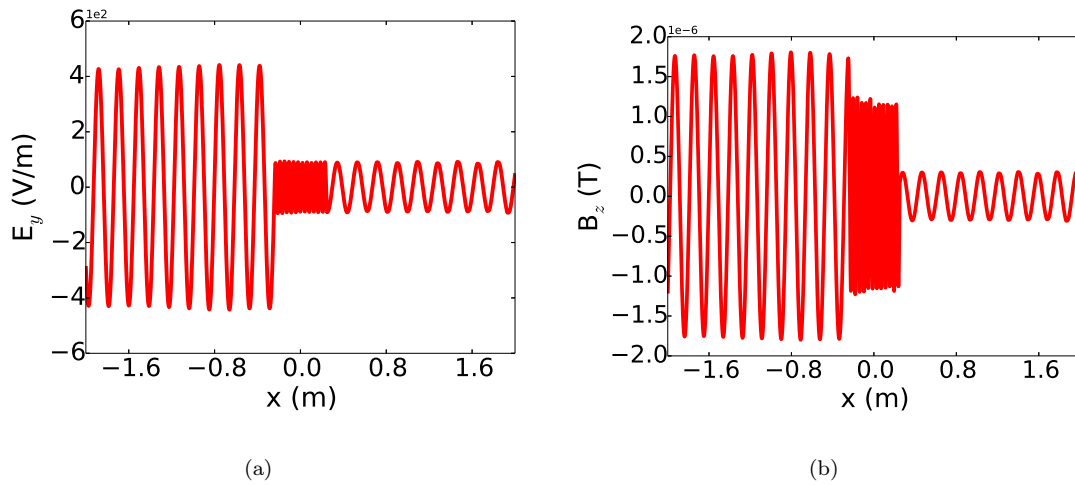


Fig. 8 The (a) y component of electric field and the (b) z component of the magnetic field of the EM wave of frequency 1.6 GHz traveling in a domain with plasma slab of thickness 0.3 m. The slab starts from $x = -0.15$ m. A background magnetic field of $B_{0x} = 1$ T is applied in the domain. The wave propagates through the plasma as a Whistler wave.

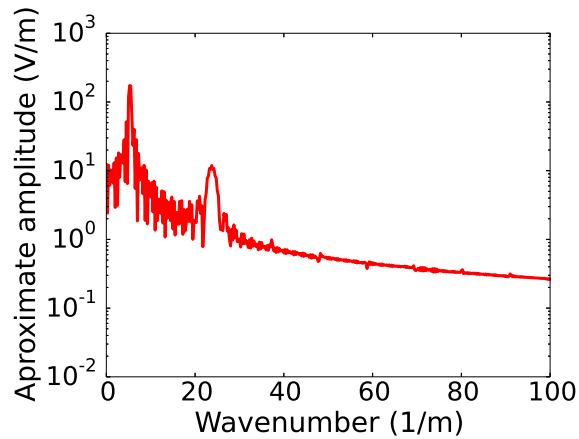


Fig. 9 The wavenumber of the plane wave in neutral fluid and plasma.

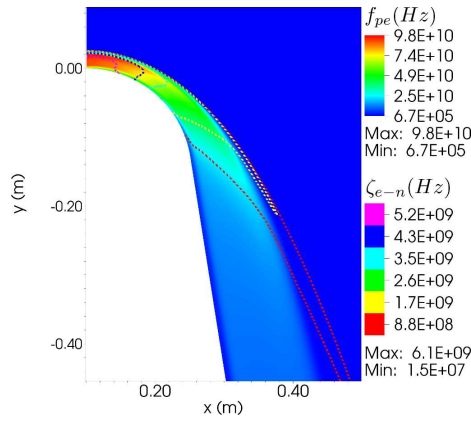
wave in the neutral zone and the second peak corresponds to the wave in the uniform plasma. Note that the amplitude does not match with the values shown in Fig.8 since the exact wave numbers 5.33 and 23.89 were not resolved by the grid. A more refined grid is required to represent the wave numbers of interest, in which case, the spectral amplitude will match the amplitude of the waves in the simulation.

IV. Electromagnetic wave propagation over the RAM C

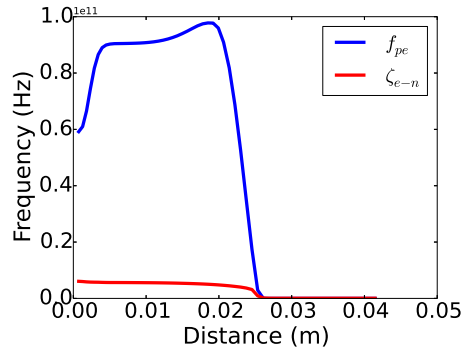
A. Blackout

In the Eqs.(18)–(20), the advection and viscous diffusion occur on much larger time scales when compared to the time scale of the plasma oscillations and EM wave. For instance, the smallest advection and diffusion time scales in the stagnation region are 4.8×10^{-6} and 8.9×10^{-6} s respectively. Whereas the plasma oscillations occur on the time scale of 1.1×10^{-11} s. In the aft region ($y=-1.25\text{m}$), the minimum advection and diffusion times are 2.73×10^{-7} and 1.78×10^{-6} s respectively. The plasma frequency time scale is 1.01×10^{-10} s. Overall, the timescales of the advection and diffusion are more than three orders of magnitude the plasma oscillation time scale. Hence, the advection and the viscous diffusion terms were neglected. Note that the length scale used in the estimation of time scales was the average edge length of the local cell. The collision term in Eqs.(18)–(20) is neglected too as the collision frequency[26, 27] of the electrons and neutrals is less than an order of magnitude the plasma frequency. Figure 10 shows the comparison. The contour flood in Fig.10(a) represents the plasma electron frequency and the contour lines show the electron neutral collision frequency. In the present simulation, the electron neutral collision frequency is highest among the collisions of the remaining species. The highest values of the frequencies are seen near the stagnation region, where the densities are high. The contours clearly show that plasma frequency is higher than the collision frequency everywhere within the plasma layer. Also, a line plot comparison along the stagnation line is shown in Fig.10(b) to get a better picture of the comparison of magnitudes.

The wave reflection by the plasma layer of the RAM C is shown in Fig.11. The frequency of the plane wave originating at the top boundary is 1.6 GHz. The wave components at the top boundary are $E_x = ca_0 \sin(2\pi ft)$, $B_z = E_y/c$ and the remaining components are equal to zero. Figures 11(a) and 11(b) represent the x,y components of the electric field. Figure 11(c) represents the z-component of the magnetic field. The contour flood shows the amplitudes of the wave. The dashed contour lines represent the plasma frequency. It can be clearly observed from the figures that the wave is completely reflected by the plasma layer once the plasma frequency is 1.6 GHz. Note that the flood contour levels are limited between peak positive and negative amplitudes of the



(a)



(b)

Fig. 10 Comparison of the plasma electron frequency ω_{pe} and the collision frequency of electrons with neutrals ζ_{e-n} . (a) contour lines of ζ_{e-n} and the contour flood of ω_{pe} . (b) Line plot of the frequencies along the stagnation line.

original wave, in order to make the wave visible. The wave's amplitude increases by about 10 times at the edge of the plasma layer due to the resonance of the evanescent wave.[16] The amplified wave propagates along the plasma layer's edge.

B. Magnetic window whistler mode

The magnetic field was applied on the surface near to the nosecap using a current carrying coil of radius 0.1 m centered at (0.15, -0.15). The current was 1.5×10^5 A. In practice a permanent magnet would be used to generate the field. The magnetic field lines colored in magnitude can be seen in all of the subplots of Fig.12. The maximum field strength available on the RAM C surface is 0.77 T while the value is around 0.125T at the the edge of the plasma layer where significant propagation

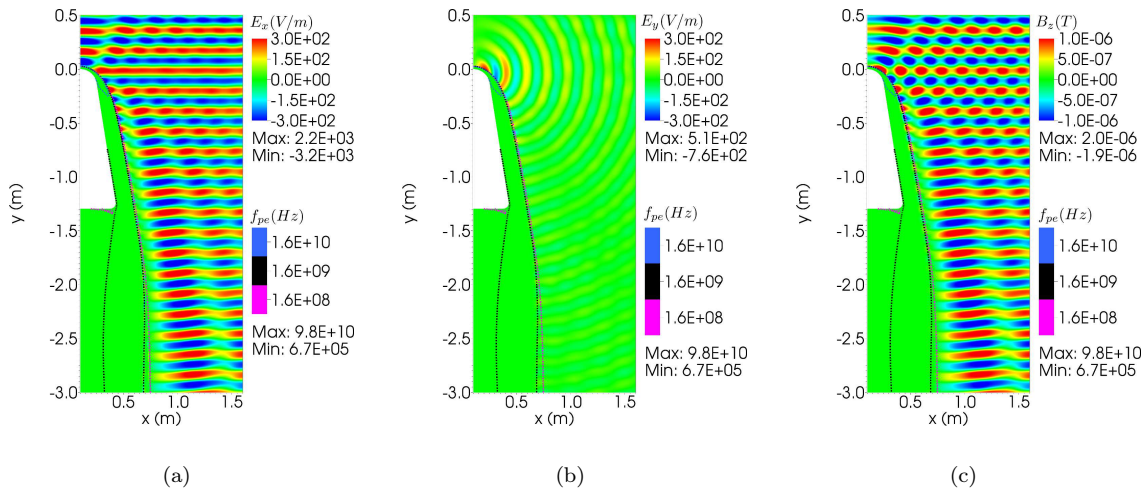


Fig. 11 EM wave reflection in the plasma layer of RAM C. (a) x component of the electric field, (b) y component of the electric field, and (c) z component of the magnetic field. The contour lines represent the plasma electron frequency.

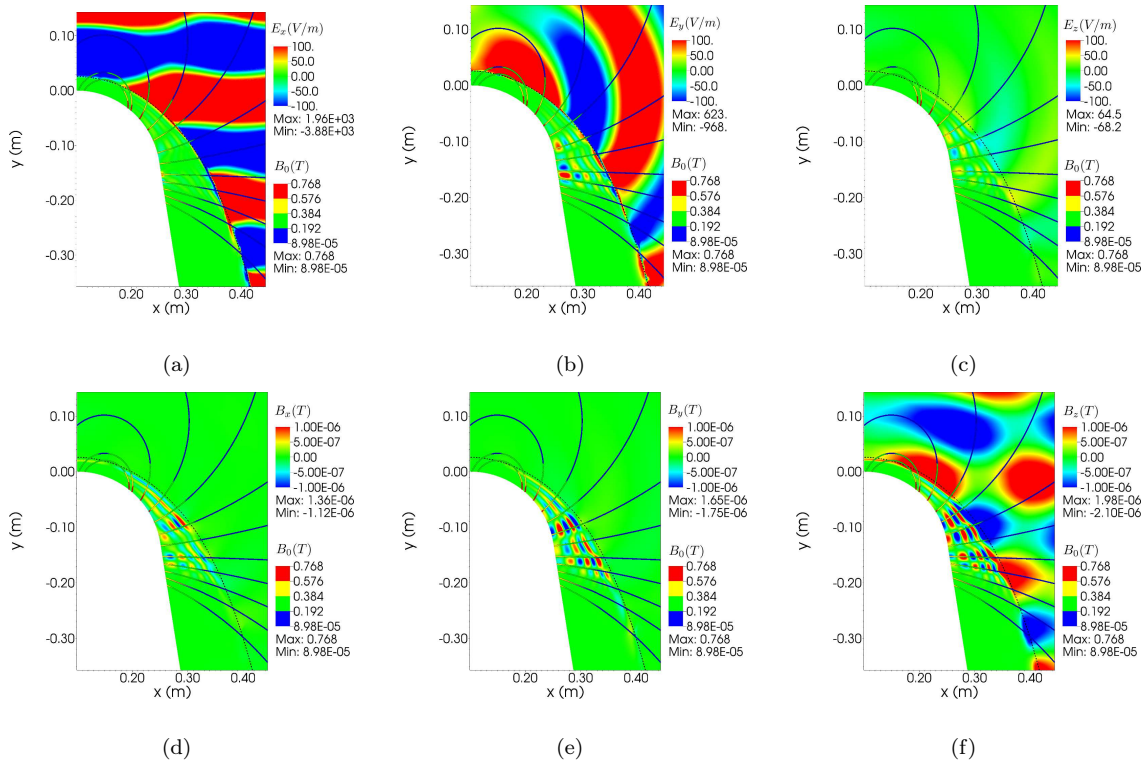


Fig. 12 EM wave propagation in whistler mode into the plasma layer of RAM C. The imposed magnetic field is shown by the streamlines. The three components of the electric and magnetic field are shown by the contour floods of (a), (b), (c), (d), (e), (f) respectively. The black dashed contour line corresponds to the plasma electron frequency of 1.6 GHz.

of wave occurs. These magnetic field strengths are slightly large, however, many hypersonic vehicles of interest will actually have a considerably smaller plasma density and thus require a much weaker field to allow whistler wave propagation - this situation described can be considered an extreme case. In addition, it's possible that using a weaker field will still allow whistler wave propagation as the evanescent waves may propagate through the outer edge of the plasma where the field is weak, then propagate as whistler waves closer to the vehicle surface. Figure 12 shows the flood contours of electric and magnetic field components of the EM wave. The cutoff frequency of plasma $f_{pe} = 1.6$ GHz is depicted by the dashed contour line. The three components of the electric and magnetic field are shown in Figs.12(a)-12(c) and Figs.12(d)-12(f) respectively. It has to be noted that, the electric field contours are limited between -100 and 100 V/m, in order to improve the visibility of the whistler wave. It is clear now that the wave signal propagates through the plasma layer in the whistler mode. The additional components arising in Fig.12 when compared to the Fig.11 are due to the circular polarization of the wave around the magnetic field lines. The circularly polarized wave propagates parallel to the magnetic field lines. Hence the angle between the wave vector and the magnetic field lines at the edge of the plasma layer plays an important role. The wave does not propagate along the field lines perpendicular to the direction of propagation. It can also be observed from the figure that the magnetic window not only allows the passage of the original electromagnetic wave, it also focuses the wave through the converging magnetic field, which is in agreement with the observations made in Ref.[38].

The ability to recover the original signal on the surface can be checked to verify that a useable signal can be obtained. The best way to do this is to find the frequency of the signal and its energy density at the surface. The frequency of the whistler wave is obtained by taking Fourier transform of the wave history recorded on the surface of RAM C. Figure 13 shows the frequency of E_y at (0.25555, -0.15829). The highest peak corresponds to a frequency of 1.6 GHz verifying that the original signal can be recovered at the vehicle surface.

In addition to the frequency match, the signal strength can also be calculated. The comparison of the energy density of the signal in the free space and that on the surface gives an idea of the signal strength. The wave's energy density is computed using Eq.32. A comparison of the electromagnetic

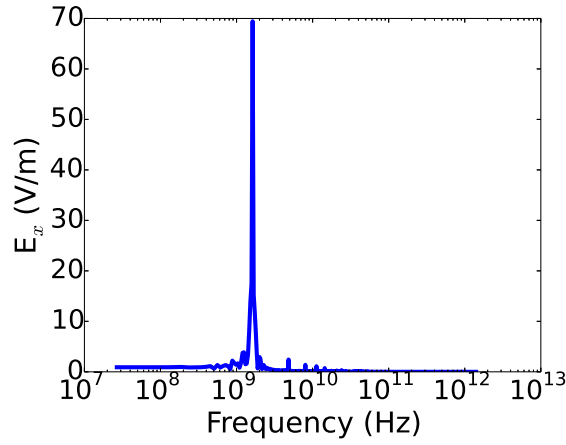


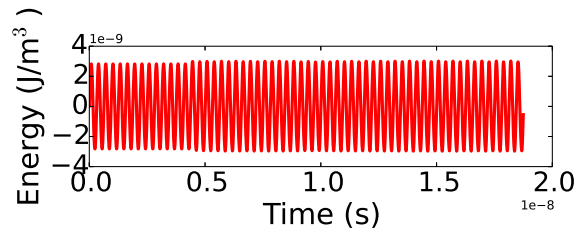
Fig. 13 Whistler wave frequency on the surface of RAM C.

energy density of the wave in the free space and that of the whistler wave on the surface of RAM C at (0.25555, -0.15829) is shown in Fig. 14. The Fig.14(a) corresponds to the wave in the free space and bottom subplot is for the Whistler wave. The slight rise in the energy of the free space wave at $t = 4.5$ ns is due to the added reflected components. It can be seen from Fig.14(b) that the whistler wave's energy is sufficient to be received by the antenna. The whistler wave's energy density is about 40% that of the original wave.

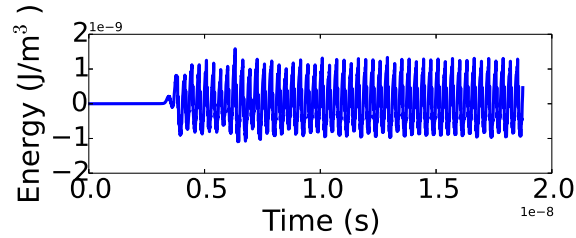
$$Q_{EM} = \frac{1}{2} \left(\epsilon_0 \vec{E} \cdot \vec{E} + \frac{1}{\mu_0} \vec{B} \cdot \vec{B} \right) \quad (32)$$

Another interesting observation made during the simulations is the amplification of the whistler wave energy density with the increase of magnetic field. For instance, increasing the coil current by 4 times generates a maximum magnetic field of 3.1 T on the surface. The strength of the magnetic field at the plasma layer's edge where whistler wave propagation occurs in this case is around 0.8 T. The wave energy density history in a magnetic window created with the increased magnetic field is shown in Fig.15. The energy density in this case is 400% of the source wave. In fact, the energy is amplified by about four times the wave's energy in the free space. As explained previously, the amplification is due to the focusing of wave along the converging field lines. This amplification could be useful in the cases where, the original signal itself is weak.

From the above feasibility analysis, it can be said that the magnetic window subjected to a realistic flight condition is capable of propagating the signal on to the vehicle's surface with energy



(a)



(b)

Fig. 14 The energy density recorded in the free space and on the surface of RAM C. The maximum magnetic field on the RAM C surface is 0.77 T and the magnetic field at the plasma layer's edge where the wave propagates is 0.125 T. (a) Recorded in free space and (b) on the RAM C surface at (0.25555, -0.15829).

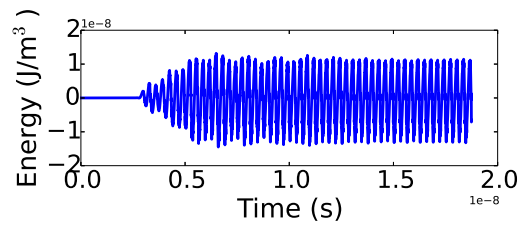


Fig. 15 The recorded energy density on the surface of RAM C at (0.258043, -0.172272). The maximum magnetic field on the RAM C surface is 3.1 T and the magnetic field at the plasma layer's edge where the wave propagates is 0.8 T.

densities ranging from 40% to 400% using magnetic fields of 0.15T and 0.8 T respectively at the edge of the plasma layer. However, the configuration can be further optimized by changing the orientation of the magnetic field lines after obtaining the plasma distributions for all the critical flight conditions in terms of angle of attack, speed and altitude.

The designer can also test other mitigation methods using the same model described in this paper. For instance, electrophilic fluid injection method can be tested by adding the additional reactions to the existing reactions set of the multi-species transport equations to establish the

reduced plasma density. The electron acoustic wave transmission can be tested by including the multi-fluid advection terms in the analysis[34] so that the electron acoustic wave is simulated. Similarly, resonant transmission can be modeled with the equations described.

V. Summary

A procedure to model and simulate the hypersonic flow and the vehicle's communication blackout is shown. The plasma density on the RAM C vehicle showed a good agreement with the reflectometer measurements from the literature. Addition of radiation losses to the reactive flow could further improve the accuracy the simulation results. The results of Maxwell equation solver of USim are validated with the analytical solution of whistler wave propagation in one dimensional plasma layer. The Whistler mode propagation of the wave on the RAM C surface is demonstrated successfully. The frequency and the energy density of the wave signal recorded on the surface of RAM C showed a good possibility of recovering the signal propagated in whistler mode. Although only the magnetic window was investigated, the same plasma model together with the solver can be used to investigate many radio blackout mitigation schemes including electron acoustic wave transmission and resonant transmission.

Acknowledgments

The authors are thankful to the financial support from AFOSR (grant numbers FA9550-12-C-0039 and FA9550-14-C-0004). The authors thank Dr. Thomas Jenkins, Dr. Ming-Chieh Lin, and Dr. David Smithe of Tech-X Corporation, for their helpful comments.

References

- [1] Bertin, J. J., "Hypersonic aerothermodynamics," *AIAA*, 1994, pp.4-5.
- [2] Meyer, J.W., Lockheed Martin Corp., Palo Alto, CA, U.S. Patent "System and method for reducing plasma induced communication disruption utilizing electrophilic injection and sharp reentry vehicle nose shaping," Publication No. US7237752 B1, filed 18 May. 2004.
- [3] Stenzel, R. L. and Urrutia, J. M., "A new method for removing the blackout problem on reentry vehicles," *Journal of Applied Physics*, Vol. 113, No. 10, 2013, 103303.

- [4] Visbal, Miguel R and Sherer, Scott E and White, Michael D, "High-Order Methods For Wave Propagation", *DTIC Document*, 2008.
- [5] Josyula, E. and Bailey, W.F., "Governing equations for weakly ionized plasma flowfields of aerospace vehicles," *Journal of spacecraft and rockets*, Vol. 40, No. 6, 2003, pp. 845–857.
- [6] Jones, W.L.Jr. and Cross, A.E., "Electrostatic-probe measurements of plasma parameters for two reentry flight experiments at 25000 feet per second," *NASA TN D-6617*, Washington, D.C., Feb 1972.
- [7] Grantham, W. L., "Flight results of a 25000-foot-per-second reentry experiment using microwave reflectometers to measure plasma electron density and standoff distance," *NASA-TN-D-6062, L-7107*, Washington, D.C., Dec 1970.
- [8] Leer, V.B., "Towards the ultimate conservative difference scheme. V. A second-order sequel to Godunov's method," *Journal of computational physics*, Vol. 32, No. 1, 1979, pp. 101–136.
- [9] Einfeldt, B., "On Godunov-type methods for gas dynamics", *SIAM Journal on Numerical Analysis*, Vol. 25, No. 2, 1988, pp. 294–318.
- [10] Jenkins, T. G., Austin, T. M., Smithe, D. N., Loverich, J. and Hakim, A. H., "Time-domain simulation of nonlinear radiofrequency phenomena", *Physics of Plasmas*, Vol. 20, No. 1, 2013, 012116.
- [11] Kumar, Harish and Mishra, Siddhartha, "Entropy stable numerical schemes for two-fluid plasma equations", *Journal of Scientific Computing*, Vol. 52, No. 2, 2012.
- [12] Loverich, John and Hakim, Ammar and Shumlak, Uri, "A discontinuous Galerkin method for ideal two-fluid plasma equations", *Communications in Computational Physics*, Vol. 9, No. 2, 2011
- [13] Hodara, H, "The use of magnetic fields in the elimination of the re-entry radio blackout", *Proceedings of the IRE*, Vol. 49, No. 12, 1961.
- [14] Takahashi, Yusuke and Yamada, Kazuhiko and Abe, Takashi, "Prediction Performance of Blackout and Plasma Attenuation in Atmospheric Reentry Demonstrator Mission", *Journal of Spacecraft and Rockets*, 2014.
- [15] Takahashi, Y., Yamada, K. and Abe, T., "Examination of Radio Frequency Blackout for an Inflatable Vehicle During Atmospheric Reentry," *Journal of Spacecraft and Rockets*, Vol. 51, No. 2, pp. 430-441, 2014.
- [16] White, R. B. and Chen, F. F., "Amplification and absorption of electromagnetic waves in overdense plasmas", *Plasma Physics*, Vol. 16, 1974, pp. 565–587.
- [17] Merritt, E. C., Moser, A. L., Hsu, S. C., Loverich, J. and Gilmore, M., "Experimental characterization of the stagnation layer between two obliquely merging supersonic plasma jets", *Bulletin of the American Physical Society*, Vol. 58, 2013.

- [18] Shumlak, U. and Loverich, J., "Approximate Riemann solver for the two-fluid plasma model", *Journal of Computational Physics*, Vol. 187, No. 2, 2003, pp.620–638.
- [19] Shumlak, U and Lilly, R and Miller, S and Reddell, N and Sousa, E, "High-order finite element method for plasma modeling", *Pulsed Power Conference*, 2013.
- [20] Srinivasan, Bhuvana and Hakim, Ammar and Shumlak, Uri, "Numerical methods for two-fluid dispersive fast MHD phenomena", *Communications in Computational Physics*, Vol. 10, 2011.
- [21] Gillman, E. D., Foster, J. E. and Blankson, I. M., "Review of leading approaches for mitigating hypersonic vehicle communications blackout and a method of ceramic particulate injection via cathode spot arcs for blackout mitigation", *NASA/TM-2010-216220*, 2010.
- [22] Keidar, M., Kim, M. and Boyd, I., "Electromagnetic reduction of plasma density during atmospheric reentry and hypersonic flights", *Journal of Spacecraft and Rockets*, Vol. 45, No. 3, 2008, pp. 445–453.
- [23] Stenzel, R. L., "Whistler wave propagation in a large magnetoplasma," *Physics of Fluids*, Vol. 19, No. 6, 1976, pp.857–864.
- [24] Manning, R. M., "Analysis of electromagnetic wave propagation in a magnetized re-entry plasma sheath via the Kinetic equation," *NASA/TM-2009-216096*, 2009.
- [25] Zhdanov, V. M., "Transport Processes in Multicomponent Plasma," *Taylor and Francis*, Philadelphia, 2002, pp. 53–58.
- [26] Rambo, P. W. and Denavit, J. "Interpenetration and ion separation in colliding plasmas," *Physics of Plasmas (1994-present)*, Vol. 1, No. 12, 1994, pp. 4050–4060.
- [27] Rambo, P. W. and Procassini, R. J., "A comparison of kinetic and multifluid simulations of laser-produced colliding plasmas," *Physics of Plasmas (1994-present)*, Vol. 2, No. 8, 1995, pp.3130–3145.
- [28] Shashurin, A., Zhuang, T., Teel, G., Keidar, M., Kundrapu, M., Loverich, J., Beilis, I.I. and Raitses, Y., "Laboratory Modeling of the Plasma Layer at Hypersonic Flight," *Journal of Spacecraft and Rockets*, Vol. 51, No. 3, 2014, pp. 838–846
- [29] Hakim, A., Loverich, J. and Shumlak, U., "A high resolution wave propagation scheme for ideal Two-Fluid plasma equations," *Journal of Computational Physics*, Vol. 219, No. 1, 2006, pp.418–442.
- [30] Loverich, J., Zhou, S. CD., Beckwith, K., Kundrapu, M., and Loh, M., Mahalingam, S., Stoltz, P. and Hakim, A., "Nautilus: A Tool for Modeling Fluid Plasmas," *51st AIAA Aerospace Sciences Meeting including the New Horizons Forum and Aerospace Exposition*, 2013.
- [31] Kundrapu, M., Loverich, J., Beckwith, K., Stoltz, P., Keidar, M., Zhuang, T. and Shashurin, A., "Modeling and Simulation of Weakly Ionized Plasmas Using Nautilus," *51st AIAA Aerospace Sciences Meeting including the New Horizons Forum and Aerospace Exposition*, 2013.

- [32] Thoma, C., Rose, D.V., Miller, C.L., Clark, R.E. and Hughes, T.P., "Electromagnetic wave propagation through an overdense magnetized collisional plasma layer," *Journal of Applied Physics*, Vol. 106, No.4, 2009, pp. 043301
- [33] Sternberg, Natalia and Smolyakov, Andrei I, "Resonant transmission of electromagnetic waves in multilayer dense-plasma structures", *IEEE Transactions on Plasma Science*, Vol. 37, No. 7, 2009.
- [34] Mudaliar, Saba and Sotnikov, Vladimir I, "Radiation Characteristics of Antennas Embedded in a Medium With a Two-Temperature Electron Population", Vol. 60, No. 10, 2012.
- [35] Thompson, Richard Joel, "Fully coupled fluid and electrodynamic modeling of plasmas: a two-fluid isomorphism and a strong conservative flux-coupled finite volume framework", *Dissertation, University of Tennessee Space Institute*, 2013.
- [36] Johnson, Evan Alexander, "Gaussian-Moment Relaxation Closures for Verifiable Numerical Simulation of Fast Magnetic Reconnection in Plasma", *Disseration, University Of Wisconsin-Madison*, 2013.
- [37] Krall, Nicholas A and Trivelpiece, Alvin W and Gross, Robert A, "Principles of plasma physics", 1973.
- [38] Takechi, S. and Shunjiro, S., "Rf wave propagation in bounded plasma under divergent and convergent magnetic field configurations," *Japanese journal of applied physics*, Vol. 38, No. 11A, pp.1278-1280, 1999.
- [39] Blacker, T. D., William, J. B. and Tony L. E., "CUBIT mesh generation environment. Volume 1: Users manual. No. SAND-94-1100," *Sandia National Labs, Albuquerque, NM (United States)*, 1994.
- [40] Ahnert, K. and Mario M., "Odeint-Solving ordinary differential equations in C++," *arXiv preprint arXiv:1110.3397*, 2011.